Comparison and Evaluation of State of Charge Estimation Methods for a Verified Battery Model

Comparison and Evaluation of State of Charge Estimation Methods for a Verified Battery Model

Behrooz Nemounehkhah, Roberto Faranda, Kishore Akkala
Department of Energy
Politecnico di Milano
Milan, Italy
behrooz.nemounehkhah@mail.polimi.it
roberto.faranda, nagavenkata.akkala@polimi.it

Hossein Hafezi, Chethan Parthasarathy, Hannu Laaksonen
School of Technology and Innovations, Electrical Engineering
University of Vaasa
Vaasa, Finland
hossein.hafezi, chethan.parthasarathy,
hannu.laaksonen@univaasa.fi

***Abstract*—Battery Energy Storage Systems (BESS) emerged over the last decade due to their proven capabilities in mobile (e.g. electric vehicles) and stationary (e.g. smart grids) solutions. To manage a BESS and sustain its high performance over time, it is mandatory to monitor the battery states accurately. One of the most important states to monitor is battery State-of-Charge (SoC). SoC cannot be measured directly, therefore, its accurate estimation can improve the performance and the flexibility of the whole system. Additionally, the indications that battery SoC provides are used both for managing safe operation of the storage system and for extending the battery lifetime by preventing over-charging/discharging. Choosing an appropriate SoC estimation algorithm is typically a trade-off between algorithm complexity and accuracy. Different SoC estimation methods can be found in literature. Generally, these methods are evaluated considering a particular application (e.g. specific battery-cell technology and C-rate) that may not be suitable for other applications. This paper is focusing on simulating a verified battery Equivalent Circuit Model (ECM) and implementing different SoC estimation algorithms, using MATLAB Simulink®, to evaluate each algorithm's performance considering constant and dynamic current profiles. The results, obtained under different conditions, are compared to identify the advantages and constraints of each SoC estimation algorithm.**

Keywords—Battery Energy Storage Systems, Battery Equivalent Circuit Model, State-of-Charge Estimation Algorithms, Model-based State-of-Charge estimation, Coulomb Counting, Extended Kalman Filter, Unscented Kalman Filter, C-rate, Dynamic Current Profiles

I. Introduction

Developments in electric mobility and the growing trend of using Renewable Energy Sources (RES) in the last decade, have considerably increased the attention on utilizing the Battery Energy Storage Systems (BESS) since these systems are capable to store a significant amount of energy for a quite long period of time and work as complementary to RES systems [1]–[2]. Accordingly, many researchers have addressed the BESS design and performance by considering specific applications and conditions.

The studies [1] revealed that the BESS performance is dependent on several factors, such as cycle life, depth of discharge, temperature, and charge/discharge rate. Therefore, the performance can be improved if the battery states are monitored accurately and a suitable BESS control strategy is adopted. One of the important factors for BESS management is State-of-Charge (SoC) which reflects the available capacity of an electric battery relative to its total capacity. Based on the application and the battery-cell technology, different battery SoC estimation methods are proposed in literature. Comparing the results published in [3]–[8], Model-based methods are verified as robust and accurate SoC estimation techniques.

Battery models described in [8]–[9], like electrochemical, analytical, electrical, thermodynamic, and artificial intelligence-based models are capable of simulating the BESS with different accuracy and working conditions. Despite their high accuracy, all these models are not suitable for real-time SoC estimation due to the high computational effort and memory required. Electrical Models denoted as battery Equivalent Circuit Models (ECMs), are the most used models for Model-based SoC estimation [8]. ECMs provide adequate accuracy with a simple structure that makes these models easily applicable.

For better SoC estimations, accuracy and applicability must be considered, not only for the models but also for the SoC estimation algorithms. This is the main reason for existing trade-off between accuracy and complexity of the SoC estimation methods. Hence, to reach higher accuracy, more complex models and algorithms must be employed. In this study, different Model-based SoC estimation algorithms are implemented using a verified Thevenin-based second-order ECM as the reference model [10]. The performance of each algorithm is evaluated considering different operation and application conditions.

The paper is structured as follows: In Section II, the battery equivalent circuit model will be represented. In Section III, different SoC estimation algorithms will be studied in detail. In Section IV, MATLAB Simulink® simulations of the battery model integrated by different Model-based SoC estimation algorithms and the test current profiles are described. Section V is dedicated to the rigorous representation of the results of the tests and the discussions. Section VI is allocated to the conclusion and future research suggestions.

II. Battery Equivalent Circuit Model

One of the main components of the Model-based SoC estimation is the battery model. The SoC can be accurately estimated under different working conditions only if the BESS model is coherent to reality. ECMs are the most frequently employed models in electromobility studies and SoC estimations because these models are less complex than the electrochemical models and have more physical correspondence to the real battery in comparison with mathematical/analytical models. Among different ECMs that are studied in [8], the Thevenin-based Second-order Equivalent Circuit (SOEC) model is adopted for this study since this model is capable of simulating the dynamic characteristics of the BESS such as, concentration polarization and the electrochemical polarization. Fig. 1, represents the dynamic SOEC model.

The model was developed to simulate the Lithium-ion battery with Nickel-Manganese-Cobalt-Oxide (NMC) cathode and graphite anode. The battery electrolyte is a

mixture of lithium hexafluorophosphate (LiPF6) with organic solvent Ethylene Carbonate (EC) and Ethyl Methyl Carbonate (EMC) [11]. The battery cell nominal voltage and nominal capacity are equal to 3.6 V and 8 Ah, respectively. The number of the layers in the battery cell is equal to 16 and the cell weight is 157 g.

The ideal voltage source V_{OC} is used for modeling the battery open-circuit voltage. R_{int} represents the battery's internal resistance. Two RC pairs (R_1, C_1, R_2, and C_2) are used to model battery transient phenomena (hysteresis effect and polarization effect) with significant accuracy since the model is enhanced with two different time constants. Although adopting more RC pairs will increase model accuracy, it will result in an undesirable increase in the model complexity [8].

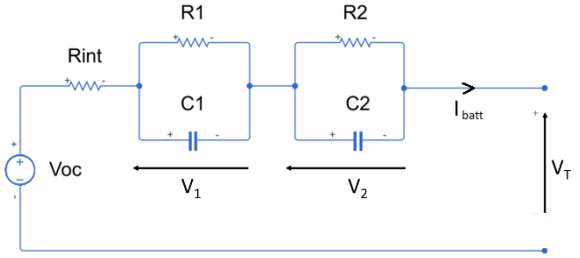

Fig. 1. Dynamic Thevenin-based second-order equivalent circuit model.

The model parameters (V_{OC}, R_{int}, R_1, C_1, R_2, and C_2) are obtained by Hybrid Pulse Power Characterization (HPPC) tests [10]. For each parameter, a lookup table is developed to model the non-linear behavior of the battery considering the effects of the SoC and operating temperature on each parameter. According to the test result and collected data, the lookup tables are characterized by breakpoints specifications equal to 0 to 100% with 10% steps for SoC and three different ambient temperature rates equal to 288.15 K, 298.15 K, and 318.15 K. V_T represents the simulated battery terminal voltage. The model equations are given by (1) – (3).

$$\dot{V}_1 = -\frac{1}{R_1 C_1} V_1 + \frac{1}{C_1} I \tag{1}$$

$$\dot{V}_2 = -\frac{1}{R_2 C_2} V_2 + \frac{1}{C_2} I \tag{2}$$

$$V_T = V_{OC} - V_1 - V_2 - (R_{int} \cdot I) \tag{3}$$

III. SoC Estimation Methods

Regarding Model-based SoC estimation, the commonly used algorithms are Coulomb Counting (CC) method and Kalman filtering methods which are combined appropriately to realize a hybrid SoC estimation technique [3].

A. Coulomb Counting Algorithm

Coulomb Counting (CC) method relies on integrating battery charging or discharging current over the time interval which provides the amount of the charge drawn from or supplied to the battery in ampere-second (As) [4]–[5]. Considering the charging or discharging operation efficiency (η) and nominal capacity (Q_{rated}), the per-unit charge lost or gained can be calculated which is used to update the initial state of charge (SoC_0). The CC equation is given in (4), where I_{batt} represents the current applied to the battery for charging or discharging.

$$SoC(t) = SoC_0 - \int_{t_0}^{t} \frac{\eta \times I_{batt}(\tau)}{Q_{rated}} d\tau \tag{4}$$

The CC method is mostly used as the main algorithm for SoC estimation since it can be easily implemented. However, the CC method suffers from a lack of accuracy due to the measurement noise which leads to accumulated errors and SoC drift. The battery capacity variations affected by operating temperature are another drawback of the CC method. Initial SoC recalibration at 100% and 0% when the battery is fully charged or discharged is a possible solution to overcome the CC method error. However, in hybrid model-based SoC estimations, the initial SoC recalibration is done more precisely using adaptive filtering algorithms such as Kalman filtering to enhance the CC method results.

B. Kalman Filter State Estimation Algorithms

Kalman Filter (KF) is an efficient tool to estimate an unknown state of a dynamic system in the presence of noise. The KF algorithm uses a Gaussian sequential probabilistic inference solution divided into two main steps denoted as prediction and correction steps to execute the state estimate and error covariance [12]. The error covariance indicates the uncertainty and error bounds for the estimated state. Due to high performance and accurate estimations achieved by KF, the algorithm has been widely used for online SoC estimation in literature. However, it should be noted that the Kalman filter also known as linear Kalman filter (LKF) is employed when the battery system is linear. Consequently, for the non-linear lithium-ion battery system adopted for this study, more precise estimators, such as Extended Kalman filter (EKF) or Unscented Kalman filter (UKF) are required.

To use the EKF and UKF estimators, the battery system state-space and output equations should be modeled in discrete time as in:

$$x_k = f(x_{k-1}, u_{k-1}) + w_k \tag{5}$$

$$y_k = g(x_k, u_k) + v_k \tag{6}$$

Where x_k is the system state vector defined based on the SOEC model equal to,

$$x_k = \begin{bmatrix} SoC_k \\ V_{1k} \\ V_{2k} \end{bmatrix} \tag{7}$$

The subscript k is used to indicate the discrete-time index. u_k is the input of the system equal to $u_k = I_{batt,k}$. w_k and v_k are the white Gaussian noise with zero mean and identified covariance matrix indicating the process noise and measurement noise, respectively. The nonlinear functions $f(x_k, u_k)$ and $g(x_k, u_k)$ are determined by the SOEC model adopted for this study. The last parameter, y_k, represents the output of the system.

The EKF uses the linearization process by implementing first-order Tylor series expansion at each time step assuming that the nonlinear functions $f(x_k, u_k)$ and $g(x_k, u_k)$, are differentiable at all operating points. Therefore, employing EKF as the state estimator for the systems with high nonlinearity will result in poor estimations. By implementing the linearization, the system state-space and output equations can be written as (8) and (9).

$$x_k = A_{k-1} x_{k-1} + B_{k-1} u_{k-1} + w_{k-1} \tag{8}$$

$$y_k = C_k x_k + D_k u_k + v_k \tag{9}$$

Although the general form of the (8) and (9) are similar to the linear system equations where LKF can be implemented, there is an important difference in the definition of A_k, B_k, C_k, and D_k matrices. These matrices are Jacobians calculated using the first-order derivative of the functions $f(x_k, u_k)$ and $g(x_k, u_k)$ with respect to x_k and u_k [15] – [16]. Considering the SOEC model adopted for this study, the aforementioned matrices are given in (10) – (13), where Ts refers to the sampling time considered for each time step, the first time constant is $\tau_1 = R_1 C_1$, and the second time constant is $\tau_2 = R_2 C_2$.

$$A_k = \frac{\partial f(x_k,u_k)}{\partial x_k}\Big|_{x_k,u_k} = \begin{bmatrix} 1 & 0 & 0 \\ 0 & e^{-\frac{Ts}{\tau_1}} & 0 \\ 0 & 0 & e^{-\frac{Ts}{\tau_2}} \end{bmatrix} \tag{10}$$

$$B_k = \frac{\partial f(x_k,u_k)}{\partial u_k}\Big|_{x_k,u_k} = \begin{bmatrix} \frac{-\eta Ts}{Q_{rated}} \\ R_1\left(1 - e^{-\frac{Ts}{\tau_1}}\right) \\ R_2\left(1 - e^{-\frac{Ts}{\tau_2}}\right) \end{bmatrix} \tag{11}$$

$$C_k = \frac{\partial g(x_k,u_k)}{\partial x_k}\Big|_{x_k,u_k} = \begin{bmatrix} \frac{\partial V_{OC}}{\partial SoC}\Big|_{SoC_k} & -1 & -1 \end{bmatrix} \tag{12}$$

$$D_k = \frac{\partial g(x_k,u_k)}{\partial u_k}\Big|_{x_k,u_k} = [-R_{int}] \tag{13}$$

The Unscented Kalman Filter (UKF) uses a different approach for state estimation. When Gaussian distribution is passed through the nonlinear functions $f(x_k, u_k)$ and $g(x_k, u_k)$, the resulting distribution will not be Gaussian anymore. The UKF uses the sampling technique known as the Unscented Transformation (UT) to approximate the Gaussian form of the transformed distribution with adequate accuracy to be used for state estimation [13]. UKF chooses a set of sampling points called weighted sigma points including the state mean to approximate the input Gaussian distribution. The deterministically chosen sigma points are then propagated through the nonlinear functions $f(x_k, u_k)$ and $g(x_k, u_k)$, to get the set of transformed sigma points whose weighted average and covariance will be used for state estimation and calculation of the error covariance at the next time step.

The sigma points are not chosen randomly, and the spread of the sigma points is controlled by three scaling factors denoted as Alpha (α), Kappa(k), and Beta(β) [12]. Alpha represents the spread of sigma points around the mean state value. To limit the sigma points' spread closer to the mean state value the Alpha should be set equal to smaller values in the range of $10^{-3} < \alpha \leq 1$. Additionally, the spread of the sigma points around the mean state value is affected by the square root of the scaling factor Kappa. Kappa value typically ranges $0 \leq k \leq 3$, such that smaller values indicate closer spread to mean state value. Beta, which includes information of the state distribution, is used to modify the weights of the transformed sigma points. As Gaussian distribution is considered for the state estimation implemented in this study, the scaling factors Alpha, Kappa, and Beta are optimally set equal to 10^{-2}, 0, and 2, respectively, to enable UKF track only a single peak in the probability distribution of the state, and to increase the accuracy of the state estimation algorithm.

Both EKF and UKF use the present state of the system ($\hat{x}_0^+$) and the error covariance (P_0^+), which identifies the precision of the initial state data, to initialize the state estimation process at time step zero. The accuracy of the initialization data will increase the robustness of the estimation algorithm as the estimations converge towards real values faster. The initialization data considered in this study are given as:

$$\hat{x}_0^+ = E[x_0] = [SoC_0, 0, 0] \tag{14}$$

$$P_0^+ = E[(x_0 - \hat{x}_0^+)(x_0 - \hat{x}_0^+)^T] \tag{15}$$

$$= diag[10^{-3}, 10^{-2}, 10^{-2}]$$

The notation "^" is used to indicate the estimated values and the superscripts "+" and "T" are indicating the posterior estimates and matrix transpose, respectively. Following the initialization step, the EKF runs the recursive sequential probabilistic inference with three prediction steps and three correction steps described in [12] –[14] , where Q_W and R_v are the covariance matrices of the white Gaussian noises w_k and v_k, respectively, given by (16) and (17) considering the conditions assumed in this study.

$$Q_W = diag([\,10^{-8}\,]) \tag{16}$$

$$R_v = [\,1\,] \tag{17}$$

The detailed recursive state estimation calculations for UKF is also described in [12] – [14]. The UKF state estimation is based on sequential probabilistic inference which consists of four main steps of initialization, sigma points computation, state prediction, and measurement update. The major part of the UKF state estimation, such as sigma point computations, weight assigning to each sigma point, propagating the sigma points through the nonlinear functions, and computing the new Gaussian mean and covariance from the transformed points are all performed by UT [13].

In comparison to EKF, which uses only one point (the mean of the Gaussian distribution) for the linearization, the UKF benefits from weighted sigma points that can model the state distribution with higher accuracy. Consequently, the UKF can be employed when the system is highly nonlinear, the functions $f(x_k, u_k)$ and $g(x_k, u_k)$, are not differentiable at all operating points, or it is not possible to calculate derivatives precisely. Using the limited number of deterministic sigma points makes the UKF computationally less complex than other adaptive filters such as Particle Filter (PF). However, using sigma points can be considered as a drawback in comparison to EKF when computational and memory constraints exist.

IV. Battery Model Simulations and Current Test Profiles

MATLAB Simulink® is used to implement the SOEC model and the SoC estimation algorithms within the model-based SoC estimation structure described in [3]. The model is developed considering the mathematical equations given in (1)-(3). For each parameter in the model *(V_{OC}, R_{int}, R_1, C_1, R_2,* and *C_2)* a lookup table is built using the experimental data from the HPPC test. Ambient temperature and current SoC is used as characterizing inputs for each lookup table. Cubic spline algorithm is selected to extract the value of each model parameter based on the SoC and temperature.

The accuracy of the simulated battery model adopted for this study is verified by comparing the model terminal voltage (V_T) with the experimental data collected by measuring the

real battery terminal voltage running the HPPC test at different ambient temperatures. It is observed that the model adopted for this study is coherent to the real battery and performs with adequate accuracy. The verification results at a temperature equal to 298.15 K and $SoC_0 = 100\%$ is shown in Fig. 2.

The CC algorithm has been developed by sampling the battery current (I_{batt}) considering sampling time Ts= 0.1 s, and using a memory block to store the current SoC value to be used as the initial State-of-Charge (SoC_0) in the next time step. The efficiency (η) is set equal to 97% for both charging and discharging processes in this study.

The battery system state-space and output equations are modeled using Simulink functions. These functions specify the state transition and measurement functions in EKF and UKF blocks, that are simulated using Simulink Control System Toolbox. The terminal voltage of the simulated battery model (V_T) with random noise is used as the system measured output required by EKF and UKF state estimators.

The parameters for EKF and UKF blocks are tuned to achieve the highest accuracy at HPPC test conditions. The value of these parameters is reported in (14)-(17). The process and measurement noise are both considered additive in this study and the relative covariances are considered time-invariant.

Each SoC estimation structure is tested considering constant C-rates and dynamic current profiles. Each test is repeated for three temperatures equal to 288.15 K, 298.15 K, and 303.15 K. The results are compared to the reference SoC, which is obtained from the ideal integration of the battery loading current, to verify the estimation accuracy. The testing dynamic and constant current profiles defined considering both electromobility and RES application requirements are shown in Fig. 3.

The current profiles include HPPC test performed at a current rate equal to 1C, Dynamic Stress Test (DST) performed at a current rate equal to 0.5C, Federal Urban Driving Schedule (FUDS) test for batteries implemented in electric vehicles (EVs), performed at a current rate equal to 0.5C [17], battery constant C-rate cycling test performed at a current rate equal to 1C, High regime battery cycling test with partial charge/discharge profile is performed at 0.2C, and Low regime battery cycling with partial charge/discharge test performed at 0.2C. A random noise with power equal to 0.001 is added to test current profiles to realize the battery current measurement.

The time and initialization conditions defined for each test are indicated as,

- HPPC test is initialized with $SoC_0 = 100\%$, and performed for 4×10^4 s.
- DST test is initialized with $SoC_0 = 80\%$, and performed for 3.44×10^4 s.
- FUDS test is initialized with $SoC_0 = 80\%$, and run for 3.44×10^4 s.
- Battery constant C-rate cycling test is initialized with $SoC_0 = 50\%$, and run for 3.84×10^5 s.
- High regime battery cycling test is initialized with $SoC_0 = 70\%$ and run for 4.9×10^5 s.
- Low regime battery cycling test is initialized with $SoC_0 = 20\%$, and performed for 4.88×10^5 s.

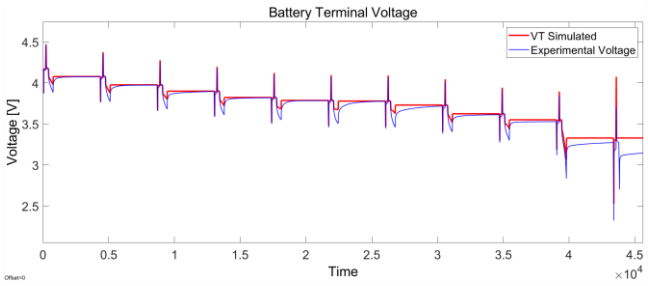

Fig. 2. Battery model verification by comparing the simulated and measured terminal voltages.

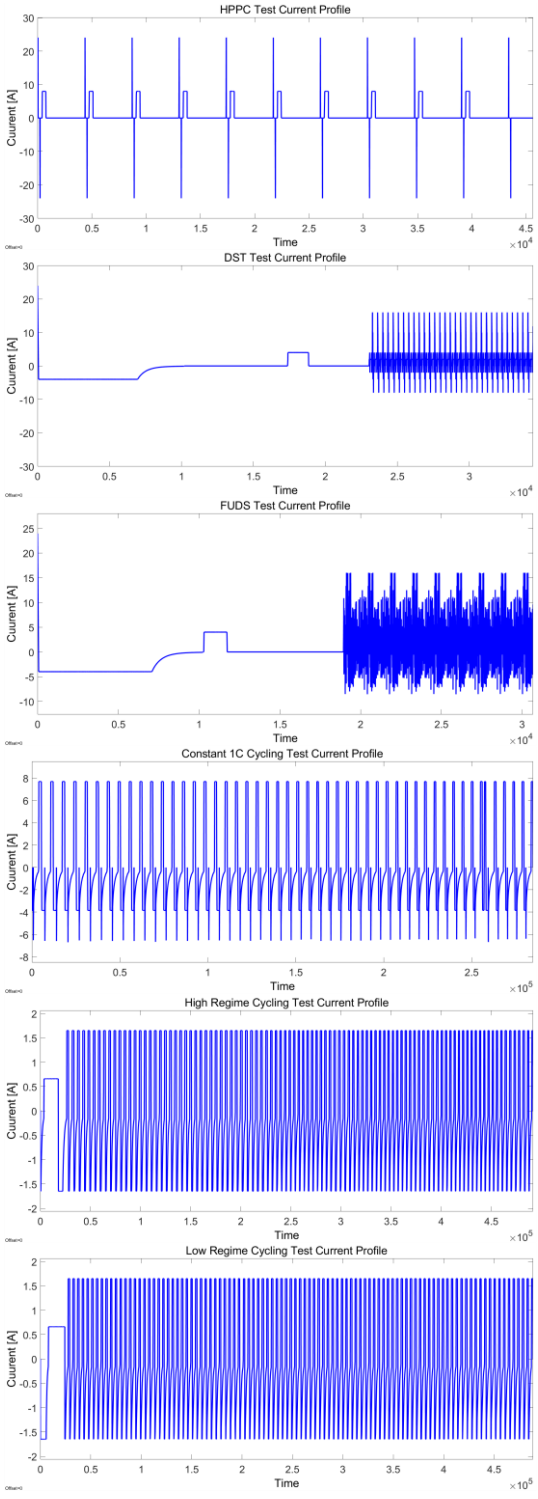

Fig. 3. Battery testing current profiles.

V. RESULTS AND DISCUSSIONS

The SoC estimation results obtained by performing the tests at 298.15 K are represented in Fig. 4. The estimation error and error mean are shown in Fig. 5. The results of each test are reported in percentage considering C-rates, time, and SoC_0 defined before. The EKF and UKF estimator parameters, such as initialization data, and the covariance matrices are tuned for optimal performance with HPPC test conditions, which resulted in estimation error within 0.5%. The tuning parameters are kept unchanged for precise comparison of EKF and UKF estimation accuracy in other test cases.

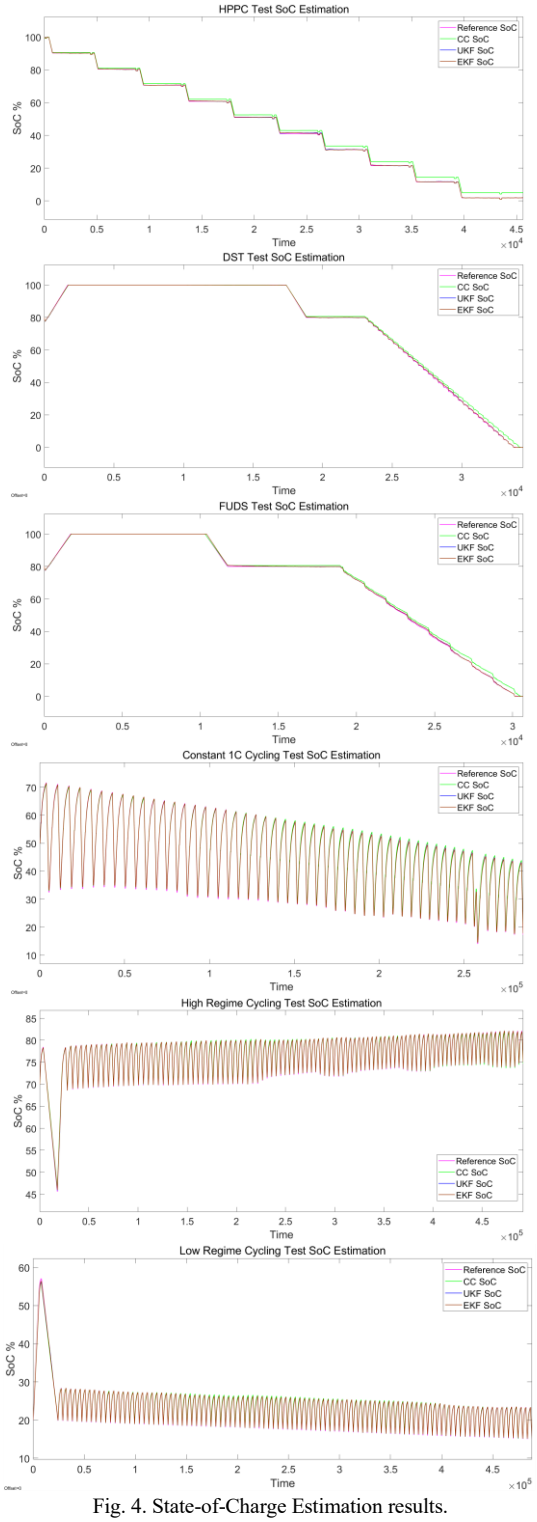

Fig. 4. State-of-Charge Estimation results.

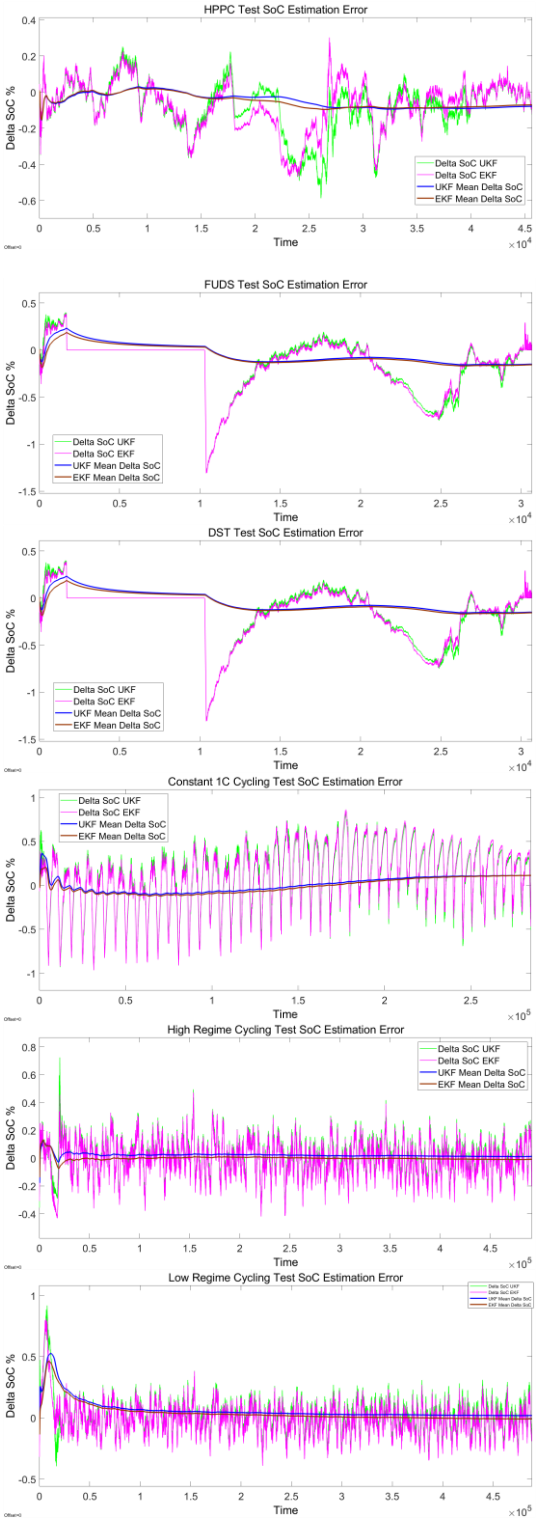

Fig. 5. State-of-Charge estimation error.

Referring to the SoC estimation results shown in Fig. 4, it can be observed that the CC algorithm suffers from accumulated error over time due to the measurement noise and charging/discharging efficiency. The error causes a non-negligible drift compared to reference SoC. According to the results, both EKF and UKF algorithms are performing with high accuracy and slight differences.

The HPPC test estimation error shown in Fig. 5, reveals that in the time interval between 1.5×10^4s, and 2.8×10^4s, corresponding to SoC range between 60% to 31% the UKF performs with higher accuracy since the model terminal

voltage profile is flat in this interval and the sigma point sampling technique employed by UKF is more efficient.

According to the results, error bound is not constant for all the test conditions. Referring to the FUDS test results shown in Fig. 5, it can be observed that the estimation error rises to 1.3% when the discharge process starts once the battery is fully charged and converges to smaller values through the time.

The estimation error bounds observed through the tests performed at three ambient temperature rates equal to 288.15 K, 298.15 K, and 303.15 K are represented in Table I, show that temperature variation does not affect the battery model and the SoC estimators' performance. However, more tests are required to verify system performance at different operating temperatures.

It should be noted that for the battery system adopted in this study, the EKF state estimator performs with sufficient accuracy and requires less computational effort. Thus, for similar battery systems with low nonlinearity, the EKF estimator can be the correct choice considering the trade-off between algorithm complexity and accuracy described earlier.

TABLE I. STATE-OF-CHARGE ESTIMATION ERROR AT DIFFERENT TEST CONDITIONS AND AMBIENT TEMPERATURE

Battery Tests	**Maximum Soc Estimation Error Percentage (%)**					
	288.15 K		***298.15 K***		***303.15 K***	
	EKF	***UKF***	***EKF***	***UKF***	***EKF***	***UKF***
HPPC	0.44	0.49	0.47	0.58	0.48	0.58
DST	0.77	0.80	0.83	0.85	0.84	0.85
FUDS	0.39	0.40	0.38	0.40	0.38	0.39
Constant Cycling at 1C	0.94	0.93	0.97	0.96	0.97	0.97
High Regime Cycling	0.5	0.71	0.47	0.72	0.47	0.72
Low Regime Cycling	0.83	0.91	0.81	0.91	0.80	0.91

VI. CONCLUSION

According to the results obtained through different tests performed in this study, it can be concluded that the battery model physical correspondence to the real battery has a significant effect on the model-based SoC estimation accuracy. Comparing the EKF and UKF state estimators for the (NMC) Lithium-ion SOEC battery model, it is highlighted that the UKF is not necessarily the best solution to address the trade-off between algorithm complexity and accuracy since the EKF performance is better with respect to the low computational effort. However, for the battery systems with high nonlinear characteristics, the UKF is recommended because the linearization technique used by EKF will not be adequate to estimate SoC with acceptable accuracy [12]. For different application conditions, the tuning parameters of the EKF and UKF must be chosen considering each algorithm's specifications and constraints, to minimize the estimation error. Therefore, future research on developing a suitable technique to extract the tuning parameters for EKF and UKF is recommended. Additionally, to provide clear insight into the strength and weaknesses of each SoC estimation algorithm and to facilitate the algorithm recognition for possible applications, more test cases with different battery chemistry and ECMs are suggested for future research.

ACKNOWLEDGMENT

The work of H. Hafezi, C. Parthasarathy and H. Laaksonen were carried out in SolarX research project with financial support provided by Business Finland, 2019-2021 (grant No. 6844/31/2018).

REFERENCES

[1] H. Hesse, M. Schimpe, D. Kucevic, and A. Jossen, “Lithium-Ion Battery Storage for the Grid—A Review of Stationary Battery Storage System Design Tailored for Applications in Modern Power Grids,” Energies, vol. 10, no. 12, p. 2107, Dec. 2017.

[2] Roopali, P. Ramachandra and J. Rodrigues, "Assessment of Battery Technologies for Future of Electro-Mobility in Emerging Markets," 2018 Conference on Emerging Devices and Smart Systems (ICEDSS), Tiruchengode, 2018, pp. 117-122.

[3] J. Rivera-Barrera, N. Muñoz-Galeano, and H. Sarmiento-Maldonado, “SoC Estimation for Lithium-ion Batteries: Review and Future Challenges,” Electronics, vol. 6, no. 4, p. 102, Nov. 2017.

[4] G. S. Misyris, D. I. Doukas, T. A. Papadopoulos, D. P. Labridis and V. G. Agelidis, "State-of-Charge Estimation for Li-Ion Batteries: A More Accurate Hybrid Approach," in IEEE Transactions on Energy Conversion, vol. 34, no. 1, pp. 109-119, March 2019.

[5] I. Baccouche, S. Jemmali, B. Manai, N. Omar and N. Amara, "Improved OCV Model of a Li-Ion NMC Battery for Online SOC Estimation Using the Extended Kalman Filter", Energies, vol. 10, no. 6, p. 764, 2017. Available: 10.3390/en10060764.

[6] Huria, T., Ceraolo, M., Gazzarri, J., and Jackey, R., "Simplified Extended Kalman Filter Observer for SOC Estimation of Commercial Power-Oriented LFP Lithium Battery Cells," SAE Technical Paper 2013-01-1544, 2013, https://doi.org/10.4271/2013-01-1544.

[7] Z. Yu, R. Huai, and L. Xiao, "State-of-Charge Estimation for Lithium-Ion Batteries Using a Kalman Filter Based on Local Linearization", Energies, vol. 8, no. 8, pp. 7854-7873, 2015. Available: 10.3390/en8087854.

[8] G. Saldaña, J. I. San Martín, I. Zamora, F. J. Asensio, and O. Oñederra, “Analysis of the Current Electric Battery Models for Electric Vehicle Simulation,” Energies, vol. 12, no. 14, p. 2750, Jul. 2019.

[9] J. Meng, G. Luo, M. Ricco, M. Swierczynski, D.-I. Stroe, and R. Teodorescu, “Overview of Lithium-Ion Battery Modeling Methods for State-of-Charge Estimation in Electrical Vehicles,” Applied Sciences, vol. 8, no. 5, p. 659, Apr. 2018.

[10] Arunachala R, Parthasarathy C, Jossen A, Garche J, “Inhomogeneities in Large Format Lithium Ion Cells: A Study by Battery Modelling Approach,” ECS Transactions. 2016 Sep 15,;73(1):201-212

[11] J. Kumar, C. Parthasarathy, M. Västi, H. Laaksonen, M. Shafie-Khah, and K. Kauhaniemi, “Sizing and Allocation of Battery Energy Storage Systems in Åland Islands for Large-Scale Integration of Renewables and Electric Ferry Charging Stations,” Energies, vol. 13, no. 2, p. 317, Jan. 2020.

[12] G. Plett, Battery Management Systems, Volume II. Norwood: Artech House, 2015.

[13] I. Jokić, Ž. Zečević and B. Krstajić, "State-of-charge estimation of lithium-ion batteries using extended Kalman filter and unscented Kalman filter," 2018 23rd International Scientific-Professional Conference on Information Technology (IT), Zabljak, 2018, pp. 1-4.

[14] R. Zhang, B. Xia, B. Li, L. Cao, Y. Lai, W. Zheng, H. Wang, and W. Wang, “State of the Art of Lithium-Ion Battery SOC Estimation for Electrical Vehicles,” Energies, vol. 11, no. 7, p. 1820, Jul. 2018.

[15] F. Ciortea, M. Nemes, S. Hintea, "Graphical Interpretation of the Extended Kalman Filter: Estimating the State-of-Charge of a Lithium Iron Phosphate Cell," Advances in Electrical and Computer Engineering, vol.18, no.3, pp.29-36, 2018.

[16] Z. Cheng, J. Lv, Y. Liu and Z. Yan, "Estimation of State of Charge for Lithium-Ion Battery Based on Finite Difference Extended Kalman Filter", Journal of Applied Mathematics, vol. 2014, pp. 1-10, 2014.

[17] M. Cai, W. Chen and X. Tan, "Battery State-Of-Charge Estimation Based on a Dual Unscented Kalman Filter and Fractional Variable-Order Model", Energies, vol. 10, no. 10, p. 1577, 2017. Available: 10.3390/en10101577.

[18] M. Cai, W. Chen and X. Tan, "Battery State-Of-Charge Estimation Based on a Dual Unscented Kalman Filter and Fractional Variable-Order Model", Energies, vol. 10, no. 10, p. 1577,2017